AIP Conference Proceedings

Design and construction of an absolute precision load gauge: Theory and experiment

Cite as: AIP Conference Proceedings **2102**, 040009 (2019); https://doi.org/10.1063/1.5099759
Published Online: 08 May 2019

Kwang Yul Kim


View Online


Export Citation

ARTICLES YOU MAY BE INTERESTED IN

High-resolution defect imaging in laminate composites and honeycomb structures
AIP Conference Proceedings **2102**, 040008 (2019); https://doi.org/10.1063/1.5099758

Characterization of steel pipeline welded joints with artificial aging using TEP measurements
AIP Conference Proceedings **2102**, 040010 (2019); https://doi.org/10.1063/1.5099760

Spatially resolved acoustic spectroscopy for texture imaging in powder bed fusion nickel superalloys
AIP Conference Proceedings **2102**, 020004 (2019); https://doi.org/10.1063/1.5099708

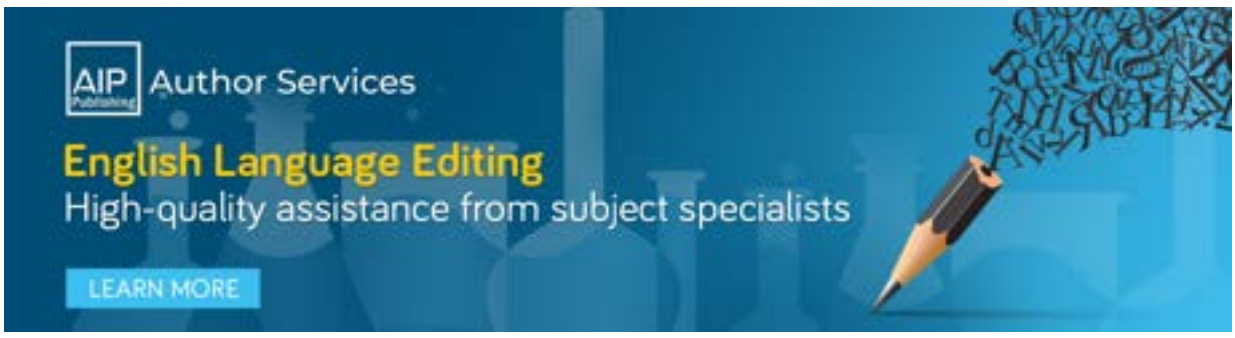

© 2019 Author(s).

Design and Construction of an Absolute Precision Load Gauge: Theory and Experiment

Kwang Yul Kim[a]

APLG LLC, 130 Fieldstone Cir, Ithaca, New York 14850, USA

[a]Corresponding author: kyk1@cornell.edu

Abstract. This paper presents (i) the formulation that calculates an applied uniaxial load on an absolute precision load gauge (APLG) by using the finite deformation theory[1,2] of an elastic solid, which was initially isotropic at strain-free state, (ii) design and construction of the APLG, and (iii) validity of the APLG by testing it under a compression machine with maximum capacity of 300 imperial tons. The load-carrying member of the APLG is a cylindrically shaped 7075 aluminum alloy with 122.61mm diameter, which can carry more than 480 metric tons of load in the elastic range without inducing plastic deformation. The vertically applied load is calculated using four measured data: a lateral dimensional change of a specimen in the horizontal direction and three travel times of horizontally propagating longitudinal, vertically polarized shear (SV) and horizontally polarized shear (SH) waves. These data can be easily measured in experiments with a great accuracy. The lateral dimensional change of the specimen is measured with a resolution of 50 nm and travel times of the sound waves are measured with accuracy better than a few parts in 100,000. The theory takes care of the linear and nonlinear elastic contributions of material behavior under finite deformation, contributing to great precision for the calculation of the applied load. The accuracy of the calculated load is better than 0.1 %. The APLG directly calculates the applied load in units of force or mass, and thus precludes the need for its calibration, providing advantages over the conventional load cells.

In the finite deformation theory the thermodynamic stress τ_{33} is calculated using the complex formulae and measured data. Dimensional changes are measured in the isothermal condition. The applied Cauchy stress σ_{33} is obtained from τ_{33} and fractional dimensional changes in lateral and vertical directions. Wave propagation is an adiabatic process that yields adiabatic second order elastic constants. Third order elastic constants obtained from the wave speed data and the dimensional change are mixed elastic constants. These adiabatic and mixed elastic constants are converted into isothermal values using the thermodynamics of finite deformation of elastic solids developed by this author.[1] Then the isothermal second order elastic compliance constant S_{33}^T and the isothermal third order elastic compliance constant S_{333}^T are calculated. Finally applied load P is expressed Several APLG applied loads are obtained under several compressive loads up to 300 imperial tons at the Test Bay of Cornell University.

INTRODUCTION

The APLG presented in this article is a high capacity load gauge that covers the load range over 10 metric tons up to over a few thousands of metric tons. In this heavy load range it is impractical to compare the applied load with the dead weight, which yields directly the applied load in force units of newton or kg. Most of the commercially available load cells are based on some sorts of arranged strain gages attached on the surface of a load carrying member and their outputs are amplified electrical quantities in proportion to the applied load. Therefore, the strain-gage based load cells are usually calibrated against the dead weight to know their real outputs. These load cells also drift with time and so they should be occasionally calibrated. Calibration could be expensive and difficult in the force range higher than one mega newton. Other type of load cells based on displacement, such as a proving ring and linear variable differential transformer (LVDT), etc., also need to be calibrated, because their outputs are not in units of force or mass. The load cells based on torque or moment also require calibration because of the same reason. To the author's knowledge, there is currently no load cell or load gauge that directly outputs the applied load in units of force or mass.

This paper addresses the short-comings of the currently available load cells in the higher load range by inventing a new load gauge that directly outputs the applied load in units of force or mass. In the past this author published several articles on the absolute stress gauge and acoustoelastcity.[1-4] This article is the extension of the author's past works. The basic idea is simple according to the linear elasticity theory. In the uniaxial homogeneous loading, say in the vertical direction 3, on an initially isotropic specimen at zero load, strain ε_{33} is linearly related to the Cauchy stress σ_{33} by the Hooke's law $\sigma_{33} = E\varepsilon_{33}$, where $E = 1/S_{11}$ is the Young's modulus of a load-carrying specimen and can

45th Annual Review of Progress in Quantitative Nondestructive Evaluation, Volume 38
AIP Conf. Proc. 2102, 040009-1–040009-12; https://doi.org/10.1063/1.5099759
Published by AIP Publishing. 978-0-7354-1832-5/$30.00

be easily and accurately obtained by measuring the longitudinal and shear wave-speeds, which also yield the Poisson's ratio $\upsilon = -S_{11}/S_{33}$. Measuring the strain ε_{33} accurately in the loading direction is much more difficult than the horizontal strain ε_{11} or ε_{22}, which can be easily and accurately measured by measuring the dimensional change of the specimen in the horizontal direction. . Here, S_{11} and S_{33} are the elastic compliance constants referred to horizontal and vertical direction, respectively. Then vertical strain ε_{33}equal to $-\varepsilon_{11}/\upsilon$, when multiplied by E, yields the Cauchy stress σ_{33}. σ_{33} multiplied by the cross-sectional area of the specimen in situ finally yields the applied load. However, a slight complication arises in this method. The Young's modulus and Poisson's ratio obtained from the longitudinal and shear wave-speeds are adiabatic constants, while the dimensional changes are measured in the isothermal condition. The adiabatic Young's modulus and Poisson's ratio can be easily converted into isothermal values by using the thermodynamics of elastic solids.[1,5] The isothermal Young's modulus and isothermal Poisson's ratio should be used to calculate the applied load. The applied load using the linear elasticity theory is fairly accurate within a few percent error but may not be accurate enough in most cases that require a higher accuracy. To improve the accuracy of the load measurement, the finite deformation theory of elastic solids is adopted to derive the formulas for the applied load. In finite deformation theory, the internal or mechanical energy contains not only harmonic potential but also anharmonic terms that contribute to the nonlinear elastic behavior of the material. The next section presents theoretical derivation of the formulas.

THEORY

Consider a load-carrying specimen that is loaded in the vertical direction 3. The Cauchy stress σ_{ij} (i,j = 1,2,3) applied in the vertical direction is specified by $\sigma_{ij}= \sigma_{33}\delta_{i3}\delta_{j3}$ and likewise the thermodynamic stress $\tau_{ij}= \tau_{33}\delta_{i3}\delta_{j3}$. The coordinates of a particle of the stressed body is said to be in the initial state and is denoted by the Cartesian coordinates **X.** The corresponding Cartesian coordinates under the stress-free zero load are denoted by vector **a**. As the stress level of the initial state **X** is arbitrary, it can include a stress free state **a** as a special case. For the sound wave propagating in the horizontal direction, say direction 1, with a wave normal **n** = [1,0,0], Christoffel equation is expressed as[6]

$$\begin{pmatrix} C_{11}^{S}(\mathbf{X};\mathbf{X}) - \rho_X V^2 & 0 & 0 \\ 0 & C_{66}^{S}(\mathbf{X};\mathbf{X}) - \rho_X V^2 & 0 \\ 0 & 0 & C_{55}^{S}(\mathbf{X};\mathbf{X}) - \rho_X V^2 \end{pmatrix} \begin{pmatrix} u_1 \\ u_2 \\ u_3 \end{pmatrix} = 0, \qquad (1)$$

where $C_{\alpha\beta}^{S}(\mathbf{X};\mathbf{X})$ are adiabatic thermodynamic elastic stiffness coefficients referenced to and evaluated at the initial state **X,** ρ_X is the density of the material at the stressed initial state and V is the sound wave speed. The former **X** and the latter **X** inside the parenthesis represent an evaluation and reference states, respectively. When the reference and evaluation states are the same in the notation of the thermodynamic elastic coefficients , it is henceforth understood that the parenthesis of the thermodynamic elastic stiffness coefficients is denoted with the single argument, as in the following examples:

$$C_{\alpha\beta}^{S\ or\ T}(\mathbf{X};\mathbf{X}) = C_{\alpha\beta}^{S\ or\ T}(\mathbf{X}), \qquad C_{\alpha\beta\gamma}^{S\ or\ T}(\mathbf{X};\mathbf{X}) = C_{\alpha\beta\gamma}^{S\ or\ T}(\mathbf{X})$$

$$C_{\alpha\beta}^{S\ or\ T}(\mathbf{a};\mathbf{a}) = C_{\alpha\beta}^{S\ or\ T}(\mathbf{a}), \qquad C_{\alpha\beta\gamma}^{S\ or\ T}(\mathbf{a};\mathbf{a}) = C_{\alpha\beta\gamma}^{S\ or\ T}(\mathbf{a})$$

The same convention applies to the compliance coefficients as

$$S_{\alpha\beta}^{S\ or\ T}(\mathbf{X};\mathbf{X}) = S_{\alpha\beta}^{S\ or\ T}(\mathbf{X}), \qquad S_{\alpha\beta\gamma}^{S\ or\ T}(\mathbf{X};\mathbf{X}) = S_{\alpha\beta\gamma}^{S\ or\ T}(\mathbf{X})$$

$$S_{\alpha\beta}^{S\ or\ T}(\mathbf{a};\mathbf{a}) = S_{\alpha\beta}^{S\ or\ T}(\mathbf{a}), \qquad S_{\alpha\beta\gamma}^{S\ or\ T}(\mathbf{a};\mathbf{a}) = S_{\alpha\beta\gamma}^{S\ or\ T}(\mathbf{a}),$$

where the superscripts *S* and T in the above equations denote adiabatic and isothermal process, respectively and subscripts $\alpha, \beta, \gamma = 1,2 \cdots 6$ are the Voigt indices.

The solution of Eq. (1) yields

$$\rho V_L^2(\mathbf{X}) = C_{11}^S(\mathbf{X}) \qquad \rho V_{21}^2(\mathbf{X}) = C_{66}^S(\mathbf{X}) \qquad \rho V_{31}^2(\mathbf{X}) = C_{55}^S(\mathbf{X}), \tag{2}$$

where $V_L(\mathbf{X}), V_{21}(\mathbf{X})$, and $V_{31}(\mathbf{X})$ denote velocities of the longitudinal wave, horizontally polarized shear (SH) wave in the direction 2 and vertically polarized shear (SV) waves in the direction 3, respectively, all propagating in the direction 1 and measured at the initial state **X.**

The dimensional change of the load-carrying member in the [100] direction is measured in an isothermal condition, while the elastic constants obtained from the wave speed measurements are adiabatic values. Isothermal elastic coefficients $C_{\alpha\beta}^T$ and $S_{\mu\nu}^T$ can be calculated from the adiabatic values by the following conversion formulae[1,5]

$$C_{\alpha\beta}^T = C_{\alpha\beta}^S - T\left(\frac{\alpha_\mu^\tau\, \alpha_\nu^\tau\, C_{\mu\alpha}^T\, C_{\nu\beta}^T}{\rho_X C_\eta}\right) \qquad (\alpha,\beta = 1,2,\cdots 6) \tag{3a}$$

$$S_{\mu\nu}^T = S_{\mu\nu}^S + T\alpha_\mu^\tau\, \alpha_\nu^\tau /(\rho_X C_\tau) \qquad (\mu,\nu = 1,2,\cdots 6), \tag{3b}$$

$$\left[S_{\alpha\beta}^T\right] = \left[C_{\alpha\beta}^T\right]^{-1}, \tag{3c}$$

where α_μ^τ is the thermal expansion coefficient at constant thermodynamic stress τ, T is the absolute temperature, $S_{\mu\nu}^T$ and $S_{\mu\nu}^S$ are respectively isothermal and adiabatic thermodynamic elastic compliance coefficients, and C_η and C_τ are the specific heat at constant Lagrange strain η_{ij} and at constant thermodynamic stress τ_{ij}, respectively. The isothermal third order elastic constants are related to the mixed order constants $C_{\alpha\beta\gamma}^M \equiv \left(\partial C_{\alpha\beta}^S/\partial\eta_\gamma\right)_T$ by[1,5]

$$C_{\alpha\beta\gamma}^T = C_{\alpha\beta\gamma}^M - TC_{3\gamma}^T\, \frac{\partial}{\partial\tau_{33}}\left(\frac{\alpha_\mu^\tau\, \alpha_\nu^\tau\, C_{\mu\alpha}^T\, C_{\nu\beta}^T}{\rho_X C_\eta}\right) \tag{4a}$$

$$S_{\alpha\beta\gamma}^T = -S_{\alpha\nu}^T S_{\beta\mu}^T S_{\gamma\lambda}^T C_{\nu\mu\lambda}^T. \tag{4b}$$

When the direction of the applied load coincides with that of the principal strain or stress, it is convenient to introduce the principal stretches defined by

$$\frac{\partial X_i}{\partial a_j} = \lambda_i\delta_{ij} \quad (i \text{ fixed}). \tag{5}$$

Note that $\lambda_1 = \lambda_2$ and $\rho_X/\rho_a = 1/(\lambda_1^2\lambda_3)$ apply to isotropic solids and also apply to cubic, hexagonal, and transversely isotropic solids when the applied loading direction coincides with one of cubic axes and the symmetry axis of hexagonal and transversely isotropic solids, respectively. For the case of $\sigma_{ij} = \sigma_{33}\delta_{i3}\delta_{j3}$ and $\tau_{ij} = \tau_{33}\delta_{i3}\delta_{j3}$

$$\lambda_1^2 = \lambda_2^2 = 1 + 2\eta_{11} = 1 + 2S_{13}^T\tau_{33} + S_{133}^T\tau_{33}^2 + \cdots \tag{6a}$$

$$\lambda_3^2 = 1 + 2\eta_{33} = 1 + 2S_{33}^T\tau_{33} + S_{333}^T\tau_{33}^2 + \cdots, \tag{6b}$$

where η_{11} and η_{33} are Lagrange principal strains in the directions 1 and 3, respectively. Let L_{a1} and ΔL_{a1} denote the specimen length in horizontal direction 1at the strain-free state and dimensional change in direction 1 under an applied load, respectively. $\lambda_1 = \lambda_2$ is given by

$$\lambda_1 = \lambda_2 = (L_{a1} + \Delta L_{a1})/L_{a1}. \tag{6c}$$

Denoting the Young's modulus of a specimen material to be $E(\mathbf{a})$ at the strain-free natural state, note that for isotropic solids at zero load

$$S_{33}^T = S_{11}^T = S_{22}^T = 1/E(\mathbf{a}) \qquad S_{13}^T = S_{12}^T = S_{23}^T \qquad S_{333}^T = S_{111}^T \,. \tag{6d}$$

Cauchy stress σ_{33} is related to thermodynamic stress τ_{33} by Murnaghan equation[7] as

$$\sigma_{33} = \frac{\rho_X}{\rho_a}\frac{\partial X_i}{\partial a_k}\frac{\partial X_j}{\partial a_l}\ \tau_{kl}\ \delta_{k3}\delta_{l3} = \lambda_1^{-2}\lambda_3\tau_{33}. \tag{7}$$

Now we introduce natural velocity W, which is defined by the original length L_{a1} at zero load in direction 1, divided by the travel time of the sound wave at a stressed state **X**. For the longitudinal waves

$$\rho_a W_L^2(\mathbf{X}) = \lambda_3\rho_X V_L^2(\mathbf{X}) = \lambda_3 C_{11}^S(\mathbf{X}) \tag{8a}$$

$$\lambda_3 C_{11}^T(\mathbf{X}) = C_{11}^T(\mathbf{a}) + \left[S_{12}^T(\mathbf{a})\left(2C_{11}^T(\mathbf{a}) + C_{111}^T(\mathbf{a}) + C_{112}^T(\mathbf{a})\right) + S_{11}^T(\mathbf{a})C_{112}^T(\mathbf{a})\right]\tau_{33} + \cdots. \tag{8b}$$

Making use of Eq. 3a and $C_{11}^S(\mathbf{a};\mathbf{a}) = \rho_a W_L^2(\mathbf{a})$, it can be seen that

$$\rho_a\left(W_L^2(\mathbf{X}) - W_L^2(\mathbf{a})\right) + \frac{TC_{1\mu}^T C_{1\nu}^T \alpha_\mu^\tau \alpha_\nu^\tau}{\rho_a C_V}(\mathbf{a}) - \frac{\lambda_3 C_{1\mu}^T C_{1\nu}^T \alpha_\mu^\tau \alpha_\nu^\tau}{\rho_X C_\eta}(\mathbf{X}) = \left[S_{12}^T(\mathbf{a})\left(2C_{11}^T(\mathbf{a}) + C_{111}^T(\mathbf{a}) + C_{112}^T(\mathbf{a})\right) + S_{11}^T(\mathbf{a})C_{112}^T(\mathbf{a})\right]\tau_{33} + \cdots. \tag{9a}$$

For shear waves, difference between isothermal and adiabatic values vanishes. Therefore,

$$\rho_a(W_{21}^2(\mathbf{X}) - W_{21}^2(\mathbf{a})) = \left[2S_{12}^T(\mathbf{a})\rho_a W_{21}^2(\mathbf{a}) + S_{12}^T(\mathbf{a})C_{111}^T(\mathbf{a})/2 + \left(S_{11}^T(\mathbf{a}) - S_{12}^T(\mathbf{a})\right)C_{112}^T(\mathbf{a})/2 - S_{11}^T(\mathbf{a})C_{123}^T(\mathbf{a})/2\right]\tau_{33} + \cdots \tag{9b}$$

$$\rho_a(W_{31}^2(\mathbf{X}) - W_{31}^2(\mathbf{a})) = \left[2S_{11}^T(\mathbf{a})\rho_a W_{31}^2(\mathbf{a}) + \left(S_{11}^T(\mathbf{a}) + S_{12}^T(\mathbf{a})\right)C_{111}^T(\mathbf{a})/4 - \left(S_{11}^T(\mathbf{a}) - S_{12}^T(\mathbf{a})\right)C_{112}^T(\mathbf{a})/4 - S_{12}^T(\mathbf{a})C_{123}^T(\mathbf{a})/2\right]\tau_{33} + \cdots. \tag{9c}$$

The two terms in Eq. 9a involving the thermal expansion coefficients and specific heats can be approximated to be linearly proportional to τ_{33}. We first notice that referring to Ref. 1, $C_\eta(\mathbf{X})$ is equal to $C_V(\mathbf{a})$ at a strain free state for isotropic and cubic solids. Its change with strain or stress is negligible within the elastic limit of solids.

$$C_\eta(\mathbf{X}) = C_V(\mathbf{a}) + \left(\frac{\partial C_\eta(\mathbf{X})}{\partial \tau_{ij}}\right)_{T;\mathbf{a}}\tau_{ij} + \cdots \cong C_V(\mathbf{a}) \tag{10a}$$

$$\alpha_1^\tau(\mathbf{X}) = \alpha_2^\tau(\mathbf{X}) = \alpha^\tau(\mathbf{a}) + \left(\frac{\partial \alpha_1^\tau(\mathbf{X})}{\partial \tau_{33}}\right)_{T;\mathbf{a}}\tau_{33} + \cdots = \alpha^\tau(\mathbf{a}) + \left(\frac{\partial S_{12}^T(\mathbf{a})}{\partial T}\right)_{T;\mathbf{a}}\tau_{33} + \cdots \tag{10b}$$

$$\alpha_3^\tau(\mathbf{X}) = \alpha^\tau(\mathbf{a}) + \left(\frac{\partial \alpha_3^\tau(\mathbf{X})}{\partial \tau_{33}}\right)_{T;\mathbf{a}}\tau_{33} + \cdots = \alpha^\tau(\mathbf{a}) + \left(\frac{\partial S_{11}^T(\mathbf{a})}{\partial T}\right)_{T;\mathbf{a}}\tau_{33} + \cdots \tag{10c}$$

$$\frac{TC_{1\mu}^{T}C_{1\nu}^{T}\alpha_{\mu}^{\tau}\alpha_{\nu}^{\tau}}{\rho_a C_V}(\mathbf{a}) = \frac{T}{\rho_a C_V(\mathbf{a})}\left[\alpha^{\tau}(\mathbf{a})\left(C_{11}^{T}(\mathbf{a}) + C_{12}^{T}(\mathbf{a}) + C_{13}^{T}(\mathbf{a})\right)\right]^2 = \frac{T\beta^2 B^{T^2}}{\rho_a C_V}(\mathbf{a}) \equiv \Delta, \tag{10d}$$

where $\beta = 3\alpha^{\tau}(\mathbf{a})$ is the volume thermal expansion coefficient and $B^T = \left(C_{11}^{T}(\mathbf{a}) + 2C_{12}^{T}(\mathbf{a})\right)/3$ is the isothermal bulk modulus at zero load natural state **a.** For simplicity of notation, hence we drop the notation (**a)** when the physical variables are evaluated at zero load state natural state **a**. In Eqs. 10a-10d we use for specific heat and temperature coefficients of $S_{11}^{T}(\mathbf{a})$ and $S_{12}^{T}(\mathbf{a})$ the values quoted in literature.[8]

Letting

$$\begin{aligned} Z_0 \equiv\ & 2S_{12}^{T}C_{11}^{T} + \Delta[2S_{12}^{T}C_{11}^{T} + (4/3)(S_{11}^{T} + 2S_{12}^{T})C_{12}^{T} + 2\beta^{-1}C_{12}^{T}(\partial S_{11}^{T}/\partial T) + \\ & 2\beta^{-1}(C_{11}^{T} + C_{12}^{T})(\partial S_{12}^{T}/\partial T)] \end{aligned} \tag{11a}$$

$$Z_1 \equiv S_{12}^{T}(1 + 2\Delta/3), \quad Z_2 \equiv S_{11}^{T}(1 + 4\Delta/3) + S_{12}^{T}(1 + 8\Delta/3), \quad Z_3 \equiv (2\Delta/3)(S_{11}^{T} + S_{12}^{T}), \tag{11b}$$

Eqs. 9a, 9b, and 9c can be written as

$$Z_1 C_{111}^{T} + Z_2 C_{112}^{T} + Z_3 C_{123}^{T} = \rho_a\,(W_L^2(\mathbf{X}) - W_L^2)/\tau_{33} - Z_0 \tag{12a}$$

$$\begin{aligned} (1/2)S_{12}^{T}C_{111}^{T} + (1/2)(S_{11}^{T} - S_{12}^{T})C_{112}^{T} - (1/2)S_{11}^{T}C_{123}^{T} = {} & \rho_a\,(W_{21}^2(\mathbf{X}) - W_{21}^2)/\tau_{33} \\ & - 2S_{12}^{T}\rho_a W_{21}^2 \end{aligned} \tag{12b}$$

$$\begin{aligned} (S_{11}^{T} + S_{12}^{T})C_{111}^{T} - (1/4)(S_{11}^{T} - S_{12}^{T})C_{112}^{T} - (1/2)S_{11}^{T}C_{123}^{T} = & \\ \rho_a\,(W_{31}^2(\mathbf{X}) - W_{31}^2)/\tau_{33} - - 2S_{11}^{T}\rho_a W_{31}^2\,. & \end{aligned} \tag{12c}$$

C_{111}^{T}, C_{112}^{T} and C_{123}^{T} in terms of τ_{33} are expressed with the following determinants:

$$D \equiv \frac{1}{8}\begin{vmatrix} Z_1 & Z_2 & Z_3 \\ S_{12}^{T} & S_{11}^{T} - S_{12}^{T} & -S_{11}^{T} \\ S_{11}^{T} + S_{12}^{T} & -S_{11}^{T} + S_{12}^{T} & -2S_{12}^{T} \end{vmatrix} \tag{13a}$$

$$E_a \equiv \frac{\rho_a}{D}\begin{vmatrix} W_L^2(\mathbf{X}) - W_L^2 & Z_2 & Z_3 \\ W_{21}^2(\mathbf{X}) - W_{21}^2 & (S_{11}^{T} - S_{12}^{T})/2 & -S_{11}^{T}/2 \\ W_{31}^2(\mathbf{X}) - W_{31}^2 & (S_{12}^{T} - S_{11}^{T})/4 & -2S_{12}^{T} \end{vmatrix} \tag{13b}$$

$$E_b \equiv \frac{\rho_a}{D}\begin{vmatrix} Z_1 & W_L^2(\mathbf{X}) - W_L^2 & Z_3 \\ S_{12}^{T}/2 & W_{21}^2(\mathbf{X}) - W_{21}^2 & -S_{11}^{T}/2 \\ (S_{11}^{T} + S_{12}^{T})/4 & W_{31}^2(\mathbf{X}) - W_{31}^2 & -S_{12}^{T}/2 \end{vmatrix} \tag{13c}$$

$$E_c \equiv \frac{\rho_a}{D}\begin{vmatrix} Z_1 & Z_2 & W_L^2(\mathbf{X}) - W_L^2 \\ S_{12}^{T}/2 & (S_{11}^{T} - S_{12}^{T})/2 & W_{21}^2(\mathbf{X}) - W_{21}^2 \\ (S_{11}^{T} + S_{12}^{T})/4 & (S_{12}^{T} - S_{11}^{T})/4 & W_{31}^2(\mathbf{X}) - W_{31}^2 \end{vmatrix} \tag{13d}$$

$$E_d \equiv \frac{\rho_a}{D}\begin{vmatrix} Z_0/\rho_a & Z_2 & Z_3 \\ 2S_{12}^{T}W_{21}^2 & (S_{11}^{T} - S_{12}^{T})/2 & -S_{11}^{T}/2 \\ 2S_{11}^{T}W_{31}^2 & (S_{12}^{T} - S_{11}^{T})/4 & -S_{12}^{T}/2 \end{vmatrix} \tag{13e}$$

$$E_e \equiv \frac{\rho_a}{D}\begin{vmatrix} Z_1 & Z_0/\rho_a & Z_3 \\ S_{12}^T/2 & 2S_{12}^T W_{21}^2 & -S_{11}^T/2 \\ (S_{11}^T + S_{12}^T)/4 & 2S_{11}^T W_{31}^2 & -S_{12}^T/2 \end{vmatrix} \tag{13f}$$

$$E_f \equiv \frac{\rho_a}{D}\begin{vmatrix} Z_1 & Z_2 & Z_0/\rho_a \\ S_{12}^T/2 & (S_{11}^T - S_{12}^T)/2 & 2S_{12}^T W_{21}^2 \\ (S_{11}^T + S_{12}^T)/4 & (S_{12}^T - S_{11}^T)/4 & 2S_{11}^T W_{31}^2 \end{vmatrix} \tag{13g}$$

$$C_{111}^T = E_a/\tau_{33} - E_{d,} \qquad C_{112}^T = E_b/\tau_{33} - E_e, \qquad C_{123}^T = E_c/\tau_{33} - E_f. \tag{14}$$

Note that all the physical variables appearing in Eqs. 13a-13g can be obtained from the four measured quantities as aforementioned with the thermal variables that can found in the literature.

Using Eq. 4b, S_{133}^T in Eq. 6a can be expressed for an isotropic solid in terms of $C_{\alpha\beta\gamma}^T$. Then,

$$\begin{aligned} \eta_{11} &= (\lambda_1^2 - 1)/2 = S_{12}^T\tau_{33} + S_{112}^T\tau_{33}^2/2 + \cdots = S_{12}^T\tau_{33} - (gC_{111}^T + hC_{112}^T + 2gC_{123}^T)\tau_{33}^2 + \cdots \\ &= (S_{12}^T - gE_a - hE_b - 2gE_c)\tau_{33} + (gE_d + hE_e + 2gE_f)\tau_{33}^2 + \cdots, \end{aligned} \tag{15}$$

where

$$g \equiv S_{12}^T\left(S_{11}^{T\,2} + S_{12}^{T\,2} + S_{11}^T S_{12}^T\right)/2, \qquad h \equiv \left(S_{11}^{T\,3} + 3S_{11}^{T\,2}S_{12}^T + 9S_{11}^T S_{12}^{T\,2} + 5S_{12}^{T\,3}\right)/2. \tag{16}$$

The last equation of Eq. 15 is a quadratic equation of τ_{33}, which can be solved with measured λ_1 or η_{11}. When η_{11} is positive under a compressive load, the negative root of $\tau_{33}$is taken by convention. The positive root of τ_{33} is taken by convention for the case of η_{11}being negative under a tensile load. $C_{111}^T, C_{112}^T,$ and C_{123}^T are then calculated via Eq. 14. $S_{333}^T = S_{111}^T$ for an isotropic solid is obtained using Eq. 4b. S_{111}^T is expressed as

$$S_{111}^T = -\left[\left(S_{11}^{T\,3} + 2S_{12}^{T\,3}\right)C_{111}^T + 12gC_{112}^T + 6S_{11}^T S_{12}^{T\,2} C_{123}^T\right]. \tag{17}$$

Finally, using Eqs. 7 and 6b, one obtains the applied load *P* on the load-carrying member of the APLG as

$$\begin{aligned} P = A_a\lambda_1^2\sigma_{33} &= A_a\lambda_3\tau_{33} = A_a(1 + 2\eta_{33})^{1/2}\tau_{33} = A_a\tau_{33}(1 + \eta_{33} - \eta_{33}^2/2 + \cdots) \\ &= A_a\tau_{33}\left[1 + S_{33}^T\tau_{33} + \left(S_{333}^T - S_{11}^{T\,2}\right)\tau_{33}^2/2\right] + \cdots \\ &= A_a\tau_{33}[1 + E(\mathbf{a})^{-1}\tau_{33} + (S_{333}^T - E(\mathbf{a})^{-2})\tau_{33}^2/2], \end{aligned} \tag{18}$$

where A_a and $E(\mathbf{a})$ are respectively the cross-sectional area and Young's modulus of the specimen at the zero load natural state. Note that for an isotropic solid $S_{33}^T = S_{11}^T, S_{13}^T = S_{12}^T,$ and $S_{333}^T = S_{111}^T$. (see Eq. 6d.)

.

EXPERIMENTAL METHODS

The schematics of the block diagrams of the experimental setup are displayed in FIG. 1. The applied load *P* is exerted on the load-carrying specimen by a 300 imperial tons capacity compression machine at the Test Bay of Cornell University. The overall pictorial view of the experimental setup is shown in FIG. 2, where it shows in the center the compression machine and the load-carrying specimen that is made of a cylindrical block of high-strength 7075 aluminum alloy with 122.61 mm cross-sectional diameter and about 360 mm height. The 7075 aluminum alloy has yield stress of over 420 MPa and the specimen can be loaded to 480 metric tons without inducing plastic deformation.

The 360 mm high circumferential side wall is shaped with four 19 mm wide flat faces, each 90 degrees apart. FIG. 3 exhibits three L, SV

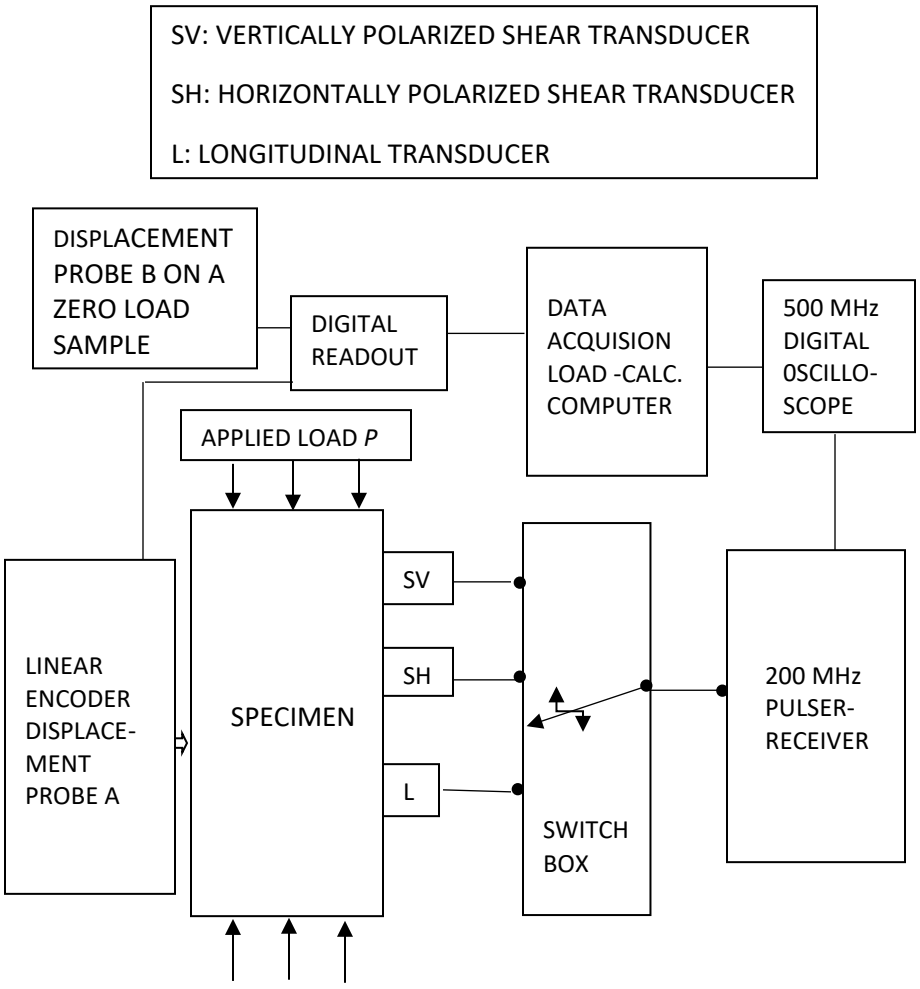

FIGURE 1. Schematics of the block diagram of the APLG experimental setup. Applied load *P* is exerted by the compressor machine.

and SH ultrasonic transducers in contact with the mid-section of the front flat face of the specimen. The ultrasonic transducers are the products of Panametrics, Inc., which are a broad band transducer with 5 MHz central frequency. As can be seen in front of the specimen in FIG. 3, the transducers are held in a jig fixed on the lower aluminum plate. The specimen is placed in the middle of the top surface of the compressor piston and stands through the central holes of upper and lower aluminum plates. Shown in FIG. 4 is a digital displacement probe A in contact with the flat surface of the rear side of the specimen with a small internal spring force. The probe A is mounted on the upper aluminum plate, which slides with little friction with four linear ball bushings along two circular bars mounted on the lower aluminum plate, which is separated from the specimen and sits fixed on the flat side bars attached on both sides of the inner column walls of the compressor. One mm thick flat microscopic glass slide placed on the front flat surface of the upper aluminum plate is in contact with the front flat surface of the specimen with a small force exerted by a tension spring on the rear side of the specimen, as shown on the bottom of FIG. 4. Saint-Venant's principal implies that the 360 mm long cylinder length, which is nearly three times the cross-sectional diameter, ensures virtually uniform stress on the midsection of about 70 mm height, where the three ultrasonic transducers and displacement probe are located.

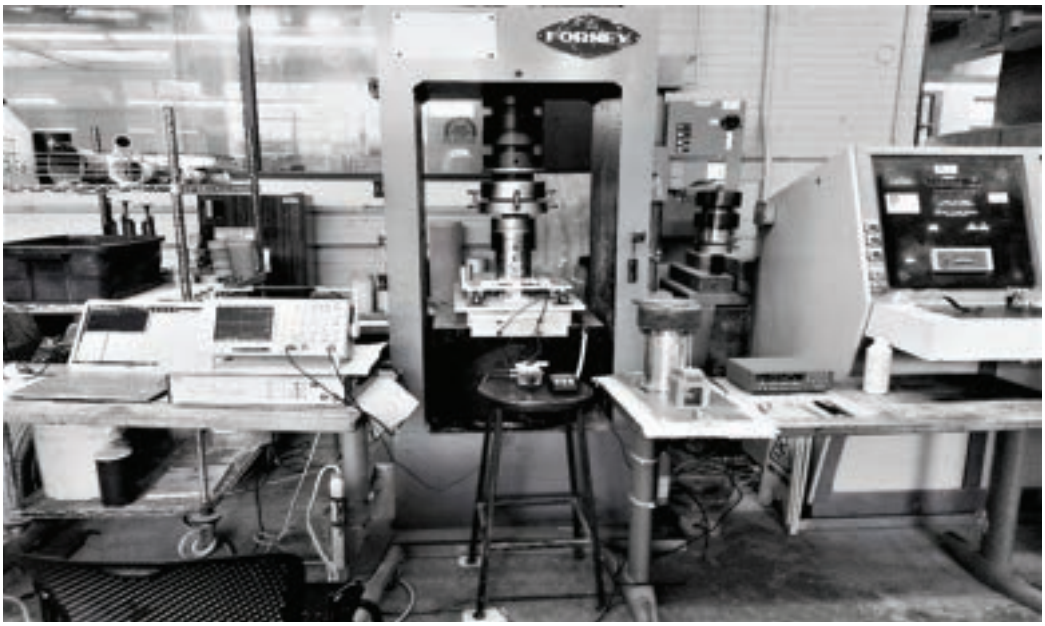

FIGURE 2. Overall view of experimental setup

The linear encoder digital displacement probe A is a product of Solartron, Inc., model LE/25/S. The dimension of the specimen under an applied load changes as the ambient temperature drifts with time. To compensate for the dimensional variations due to the temperature drift, a second probe B identical to the probe A is placed in contact with a zero load sample, which has nearly identical cross-length and is made of the same material with the specimen under the applied load. The probe B is placed next to a digital readout meter, model DR600 of Solartron, Inc. They are shown on the left side of the right table in FIG. 2. The outputs of both probes are fed into the DR600 in subtraction mode to nearly compensate for the dimensional changes due to temperature drifts. Without the second probe employed, it is desirable to minimize the temperature drift less than a few tens of one mC^{o}, as 1 C^{o} variation induces 275 nm dimensional change on the specimen. DR600 meter is also capable of displaying the output of individual probes A or B.

A 200 MHz bandwidth Panametrics pulser-receiver with 5 ns rise time is used to feed excitation pulses to three transducers via a switch box. The sound waves launched from these transducers travel across the specimen, reflect back on the opposite flat face and return to the transducers. They are amplified by the pulser-receiver and displayed on the 500 MHz Tektronix digital oscilloscope. The round trip travel times of echoed pulses are measured on the oscilloscope with an accuracy of a few parts in 100,000. The oscilloscope signals are brought into the digital computer via the GPIB bus of National Instruments, Inc. The oscilloscope and digital computer are on the left table in FIG. 2.

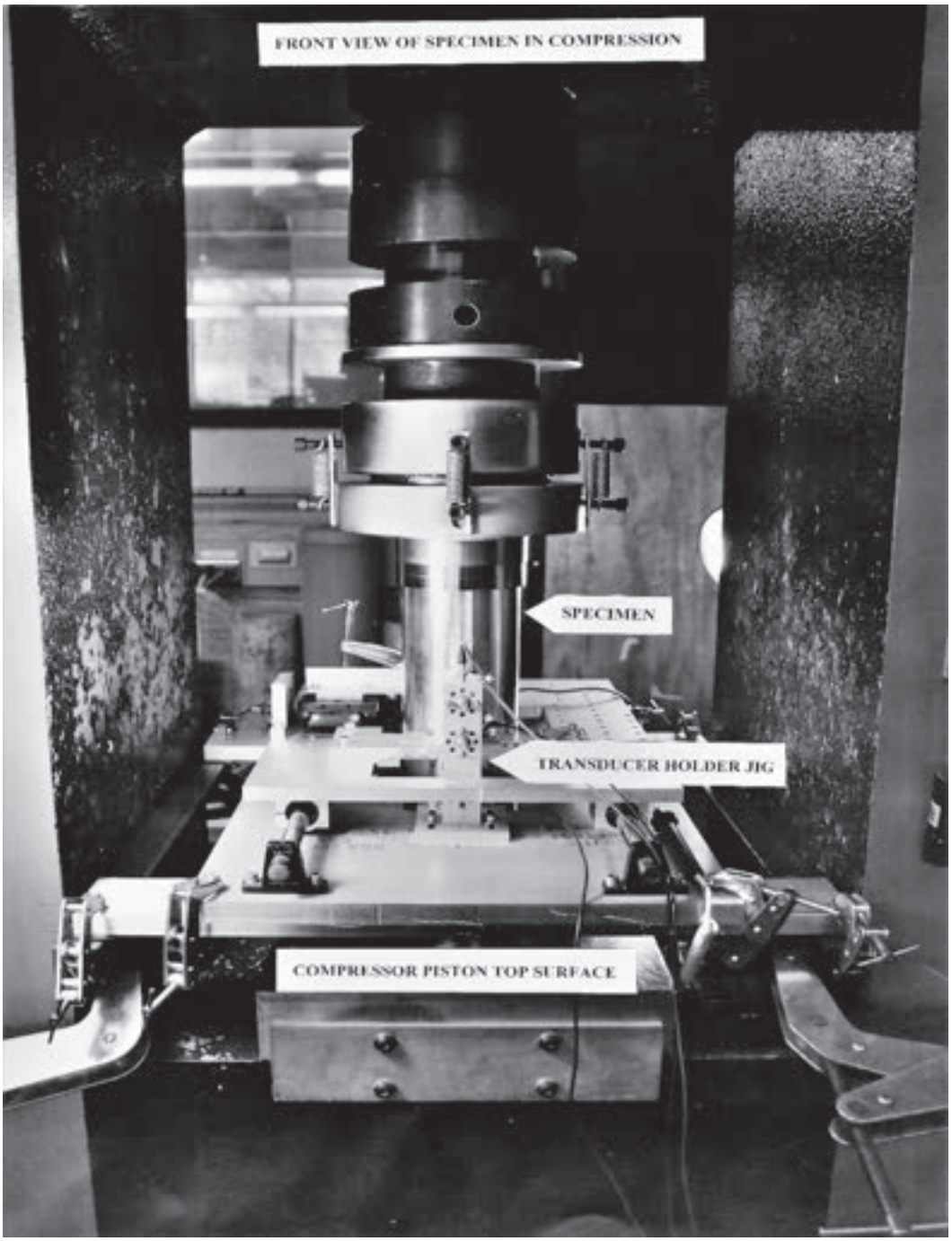

FIGURE 3. Front view of a specimen in the compression machine

Finally, the output of the digital readout of the DR600 is brought into a digital computer, which processes the four measured quantities obtained both at zero load and applied load *P* through MatLab software "CalbFree_LoadCell" written by this author using the formulae shown in the theoretical Section II. The CalbFree_LoadCell software outputs C_{11}^T, C_{12}^T, S_{11}^T, S_{12}^T, C_{111}^T, C_{112}^T, C_{123}^T, S_{111}^T, S_{112}^T, λ_1, λ_3, τ_{33}, σ_{33}, and finally the applied load *P*.

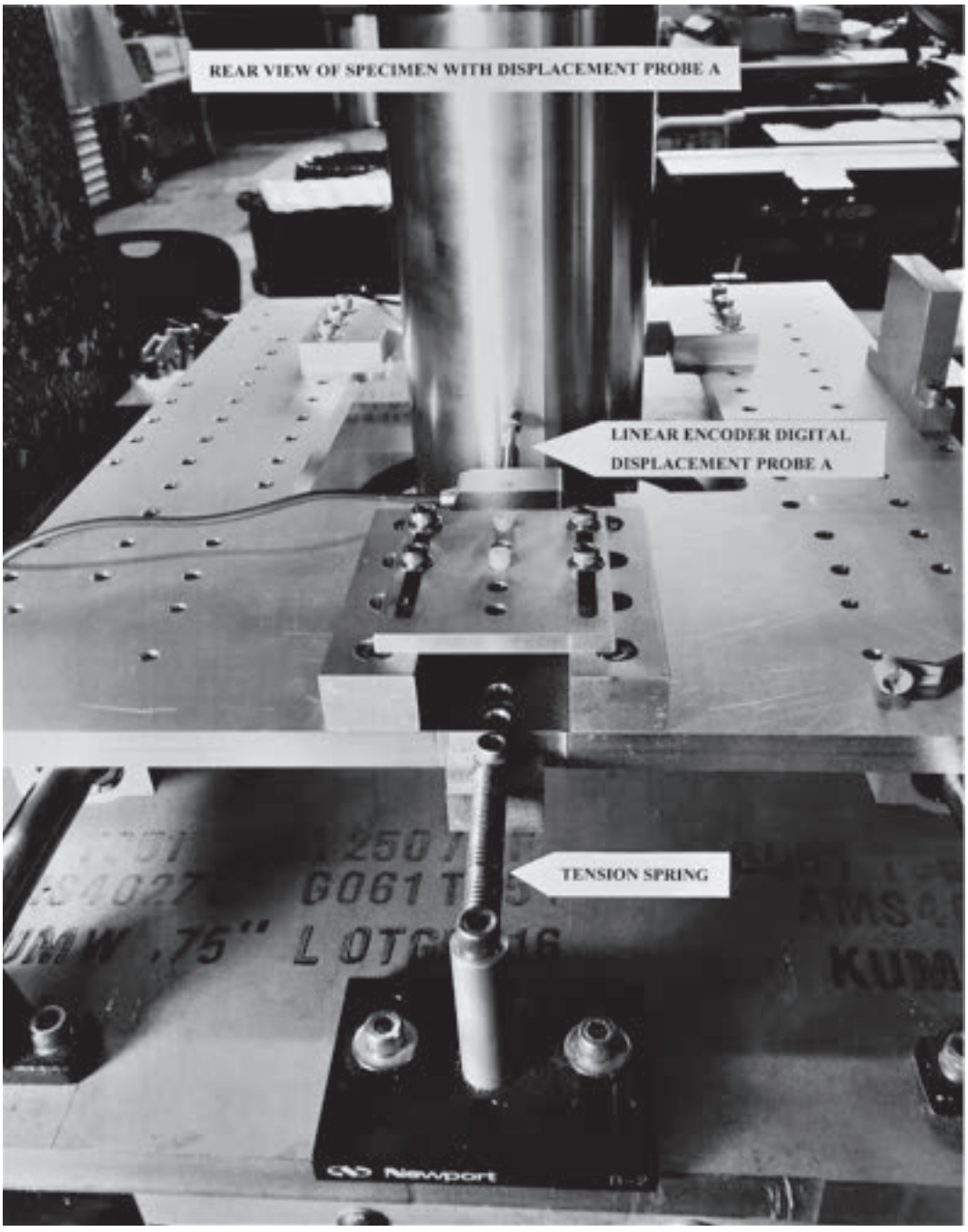

FIGURE 4. Rear view of a specimen with a digital displacement probe

COMPRESSION TEST RESULTS AND DISCUSSION

As shown in TABLE I, calculated APLG loads closely match the corresponding compressor loads with a small difference. The compressor load is only approximate, as the compressor machine did not function smoothly and its pressurizing oil medium under the piston leaked slowly during compression, and therefore it was difficult to maintain constant piston pressures. However, the close match between them provides a strong validity to the theory and

experimental methods described in this article. An ultimate test lies in comparing the output of a strain-gage based load cell recently certified by the National Institute of Science and Technology (NIST) with the APLG output under the same high capacity loading machine, whether the specimen is in tension or in compression. The second term $S_{11}^T \tau_{33}$ in the above equation contributes 0.3 % or less to the APLG load *P*. The third term $\left(S_{111}^T - S_{11}^{T\,2}\right)\tau_{33}^2/2$ provides a negligible contribution of less than 0.002 % to the APLG load *P* and may be discarded with a desired accuracy 0.01 % for the APLG load. This means that APLG load is largely determined by the $A_a \tau_{33}$ term alone with less than 1 % error.

At zero load natural state, the acoustic path length between two opposite flat faces of the specimen is 121.18 mm and the measured density ρ_a, cross-sectional area A_a and S_{11}^T are

$$\rho_a = 2808.3 \text{ kg/m}^3 \qquad A_a = = 1.1772 \times 10^{-2} m^2 \qquad S_{11}^T = 1.4048 \times 10^{-11} (Pa)^{-1}.$$

TABLE I. The values of S_{111}^T, τ_{33}, σ_{33}, and APLG Load obtained by the CalbFree_LoadCell software program at four different compressor loads

Compressor Load (Imperial Ton)	S_{111}^T ($10^{-21}(Pa)^{-2}$)	τ_{33} (MPa)	σ_{33} (MPa)	APLG Load P^* (Imperial Ton)
~ 100	3.2623	79.833	79.684	105.543
~ 150	3.2760	117.60	117.28	155.393
~ 200	3.2786	155.72	155.16	205.659
~ 250	3.3613	193.22	192.36	255.047

$^*P = A_a \tau_{33} [1 + S_{11}^T \tau_{33} + (1/2)(S_{111}^T - S_{11}^{T\,2})\tau_{33}^2 + \cdots]$

Ordinary engineering polycrystalline materials exhibit a slight anisotropy, which is difficult to characterize. During the manufacturing processes they may be heat-treated and also rolled. The rolling process induces texture in the rolled material and some of the textured materials may be characterized as possessing nearly isotropic but slightly transversely isotropic symmetry about the rolled direction. One should choose a loading direction 3 that coincides with the axis of transverse isotropy of the textured specimen. The transversely isotropic material has five second order elastic (SOE) constants, which can easily be determined at zero load natural state to calculate S_{33}^T in Eq. 18, S_{12}^T and S_{13}^T. The transversely isotropic material possesses a total of 9 third order elastic (TOE) constants, which are usually measured with a significant error. Determination of S_{333}^T via Eq. 4b is unyielding and involves a large error. However, noting that $(S_{333}^T - S_{33}^T)\tau_{33}^2/2$ in Eq. 18 makes a negligible contribution to applied load *P*, nine TOE constants of a weakly transversely isotropic but nearly isotropic specimen may be reduced to three isotropic TOE constants. Referring to Ref. 10, one replaces C_{113}^T by C_{112}^T, $C_{144}^T = C_{155}^T = C_{344}^T$ by $(C_{112}^T - C_{123}^T)/4$, C_{133}^T by C_{112}^T and C_{333}^T by C_{111}^T. For a transversely isotropic material one replaces in Eqs. 8b-16 all S_{12}^T by S_{13}^T and all S_{11}^T by S_{33}^T and derives modified equations equivalent to Eqs. 12a, 12b, and 12c involving three TOE constants C_{111}^T, C_{112}^T, and C_{123}^T. Then, τ_{33} and C_{111}^T, C_{112}^T, and C_{123}^T for a weakly transversely isotropic material can be obtained in a similar manner used in the previous section. Using Eq. 4b yields S_{333}^T in Eq. 18. With the knowledge of τ_{33}, S_{33}^T, and S_{333}^T one can finally obtain the applied load for a slightly transversely isotropic specimen. A similar approach can be extended to a slightly orthotropic specimen. The details of the texture effects on the APLG load lie outside the scope of this work and will be treated elsewhere.

A more suitable specimen material may be chosen with amorphous isotropic fused quartz, because it has higher acoustoelastic constants due to its low density (2202 kg/m^3), less than that of 7075 aluminum alloy, and because the difference between its isothermal and adiabatic values are very small due to its low thermal expansion coefficient and may be safely ignored. Therefore, fused quartz with an approximately 100 mm cross-sectional diameter may be an ideal candidate. The drawback is that it is expensive to manufacture and fabricate such a large piece of fused quartz. Another ideal specimen candidate may be a (001) oriented single crystal of silicon with an approximately 100 mm diameter cross-sectional area. The theory in Section II can be extended without difficulty to a cubic single crystalline specimen with necessary additional measurements of the sound waves propagating in the [100] and [110] directions.

The three piezoelectric ultrasonic transducers used in this experiment are a contact type, which requires a slight lateral stress on the specimen to provide a solid coupling. This coupling pressure problem can be overcome by adopting

non-contact type ultrasonic transducers, such as a dual mode EMAT (electromagnetic acoustic transducer) with a single magnet and a pancake coil described by Hirao and Ogi[9]. This type of EMAT is capable of measuring the sound speeds of L, SV, and SH waves with a single EMAT and may be ideally suited for construction of the APLG. Better accuracy and resolution in lateral displacement can be achieved by adopting a laser interferometric technique.

CONCLUSIONS

1. This work demonstrates an APLG that directly measures an applied load in units of force or mass. In a higher load range over 10 metric tons, the APLG has advantages over the conventional load cells that are based on the array of strain gages or a displacement or torque sensor, the output of which is in units of electrical quantity in proportion to the applied load. Therefore, they require calibration usually against the dead weight. Calibration in the range over one mega-newton may be expensive and difficult to perform. Their output drifts in time, requiring subsequent calibrations.
2. The formula for the applied load is established with four measured quantities: three wave-speeds of the longitudinal, horizontally polarized shear (SH) and vertically polarized shear (SV) waves propagating in the direction perpendicular to the direction of the uniaxial applied load, and a displacement of a load-carrying specimen normal to the loading direction. These four quantities can be measured with a great accuracy by adopting an up-to-date modern technique. Noncontact type EMAT(s) [9] may better replace the contact type piezoelectric transducers used in the APLG.
3. The formula Eq. 18 for calculation of the applied load can be applicable to a nearly isotropic specimen with slightly orthotropic or weakly transversely isotropic symmetry. The loading direction should be chosen so as to coincide with one of symmetry axes of the specimen. A textured specimen may possess one of these classes of symmetry. Eq. 6d applies to an isotropic specimen.
4. The texture effects and inhomogeneity of ordinary engineering polycrystalline materials can be circumvented by choosing an amorphous specimen material such as fused quartz or a single crystal such as (001) oriented silicon.

ACKNOWLEDGMENTS

This work was initiated and financed by the author. The author expresses sincere gratitude to Mr. Stephen Keast for technical assistance in the design of the APLG apparatus and Mr. James Strait for testing the APLG at the Test Bay of Cornell University.

REFERENCES

[1] K.Y. Kim, "Thermodynamics at finite deformation of an anisotropic elastic solid", *Phys. Rev. B*, **54**, 6245 (1996).
[2] K.Y. Kim and W. Sachse, "Nonlinear elastic equation of state of solids subjected to uniaxial homogenous loading", *J. Mater. Sci.* **35**, 3197 (2000).
[3] K.Y. Kim and W. Sachse, in *Handbook of Elastic Properties of Solids, Liquids, and Gases,* edited by Levy, Bass, Stern, Vol. 1, edited by A.G. Every and W. Sachse, Chap. 19, pp. 441-468, (Academic, San Diego, 2001).
[4] K.Y. Kim and W. Sachse, "The theory of thermodynamic-acoustoelastic stress gauge", *J. Appl. Phys.* **80**, 4934 (1996).
[5] R.N. Thurston, in *Handbuch der Physik*, edited by S. Flügge, in *Mechanics of Solids* VI, edited by C. Truesdell, VIa/4, pp. 109-308, (Springer-Verlag, New York, 1974).
[6] R.N. Thurston, "Effective elastic coefficients for wave propagation in crystals under stress", *J. Acoust. Soc. Am.* **37**, 348 (1965).
[7] F.D. Murnaghan, "Finite deformations of an elastic solid", *Am. J. Math*, **59**, 235 (1937).
[8] *Thermophysical Properties of High Temperature Solid Materials,* edited by Y.S. Touloukian Vol. **1-6**, Parts I and II, (Macmillan, New York, 1979).
[9] Masahiko Hirao and Hirotsugu Ogi, *EMATS for Science and Industry*: *Noncontacting Ultrasonic Measurements* (Kluwer Academic, Boston, 2003).
[10] R.F.S. Hearmon, in *Numerical Data and Functional Relationships in Science and Technology,* edited by K.-H. Hellwege and A.M. Hellwege, Landolt-Börnstein, New Series, Group III, Vol. **11** (Springer-Verlag, New York, 1979).